NANO LETTERS

pubs.acs.org/NanoLett

Letter

Wood Deformation Leads to Rearrangement of Molecules at the Nanoscale

Martin Felhofer, Peter Bock, Adya Singh, Batirtze Prats-Mateu, Ronald Zirbs, and Notburga Gierlinger*

Cite This: *Nano Lett.* 2020, 20, 2647−2653

Read Online

ACCESS | Metrics & More | Article Recommendations | Supporting Information

ABSTRACT: Wood, as the most abundant carbon dioxide storing bioresource, is currently driven beyond its traditional use through creative innovations and nanotechnology. For many properties the micro- and nanostructure plays a crucial role and one key challenge is control and detection of chemical and physical processes in the confined microstructure and nanopores of the wooden cell wall. In this study, correlative Raman and atomic force microscopy show high potential for tracking in situ molecular rearrangement of wood polymers during compression. More water molecules (interpreted as wider cellulose microfibril distances) and disentangling of hemicellulose chains are detected in the opened cell wall regions, whereas an increase of lignin is revealed in the compressed areas. These results support a new more "loose" cell wall model based on flexible lignin nanodomains and advance our knowledge of the molecular reorganization during deformation of wood for optimized processing and utilization.

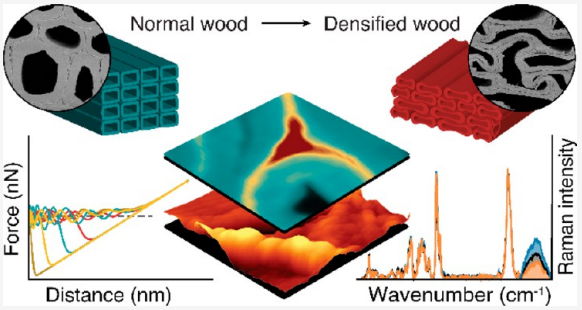

KEYWORDS: *Wood, atomic force microscopy (AFM), Raman spectroscopy, lignin, cell wall*

With increasing focus on growing global bioeconomy, the production technologies for sustainable wooden materials are rapidly advancing and include high-performance structural and multifunctional smart materials.[1−10] The strength of engineered wood was increased 8 times by delignification and re-pressing,[11] and furthermore cooling properties were reported.[12] Besides these high performance multifunctional wooden materials, also new avenues were opened by fabricating 3D shapes with tunable fiber architecture[2] and by curved mass timber structures through hygroscopic self-shaping.[4] Most of these advanced wood modifications use the unique hierarchical structure of wood as a scaffold to carry heavy loads. For the performance as well as for the functionalization and modification of wood, the microstructure (tissue and cell properties) plays a crucial role as well as the cellulose fibril network with matrix polymers (hemicellulose, lignin) and pores (water) on the nanoscale.

Thus, one key challenge in the emerging field of advanced wood functionalization is to improve nanostructural control of chemical and physical processes in the confined pore space of the cell wall and microstructure.[13] Of utmost importance are therefore methods probing *in situ* the structure, chemistry, and mechanics of the plant cell wall on the micro- and nanoscale. Among the label-free cell wall imaging techniques, atomic force microscopy (AFM) and confocal Raman microscopy have proven powerful to track topography and mechanics on the nanolevel and chemistry in context with the microstructure, respectively.[14−17] Although the two techniques are complementary in terms of length scale (micro to nanoscale) and investigated features, correlative applications are rare as they are difficult to perform on plant cell walls.[18] Furthermore, both methods are nondestructive and enable us to watch the plant cell walls *in situ*, e.g., in the stretched state[19] or enzymatically[20] or thermochemically[21] treated. Here we study for the first time the plant cell walls on the submicron and molecular levels while compressing the wood, as densification/compression is a key step in the production of many high potential and innovative wood-based materials.

Due to the honeycomb-like structure of wood, tight densification is possible and leads in a radial direction to buckling of the thin-walled earlywood cells (Figure 1a). Following one single wood cell during deformation shows compressed cell wall regions together with opened (from curved to straight) cell wall regions adjacent to cell corners (Supporting Figure 1). Under the Raman microscope these cells reveal heterogeneous uptake of water molecules within the cell wall (Figure 1b). In the opened cell wall regions a higher water content (Figure 1b, light blue, arrow) is visualized compared to the compressed area (Figure 1b, dark regions, arrowhead). The lower water content in the compressed area

Received: January 16, 2020
Revised: March 4, 2020
Published: March 20, 2020

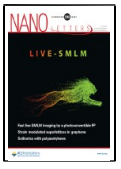

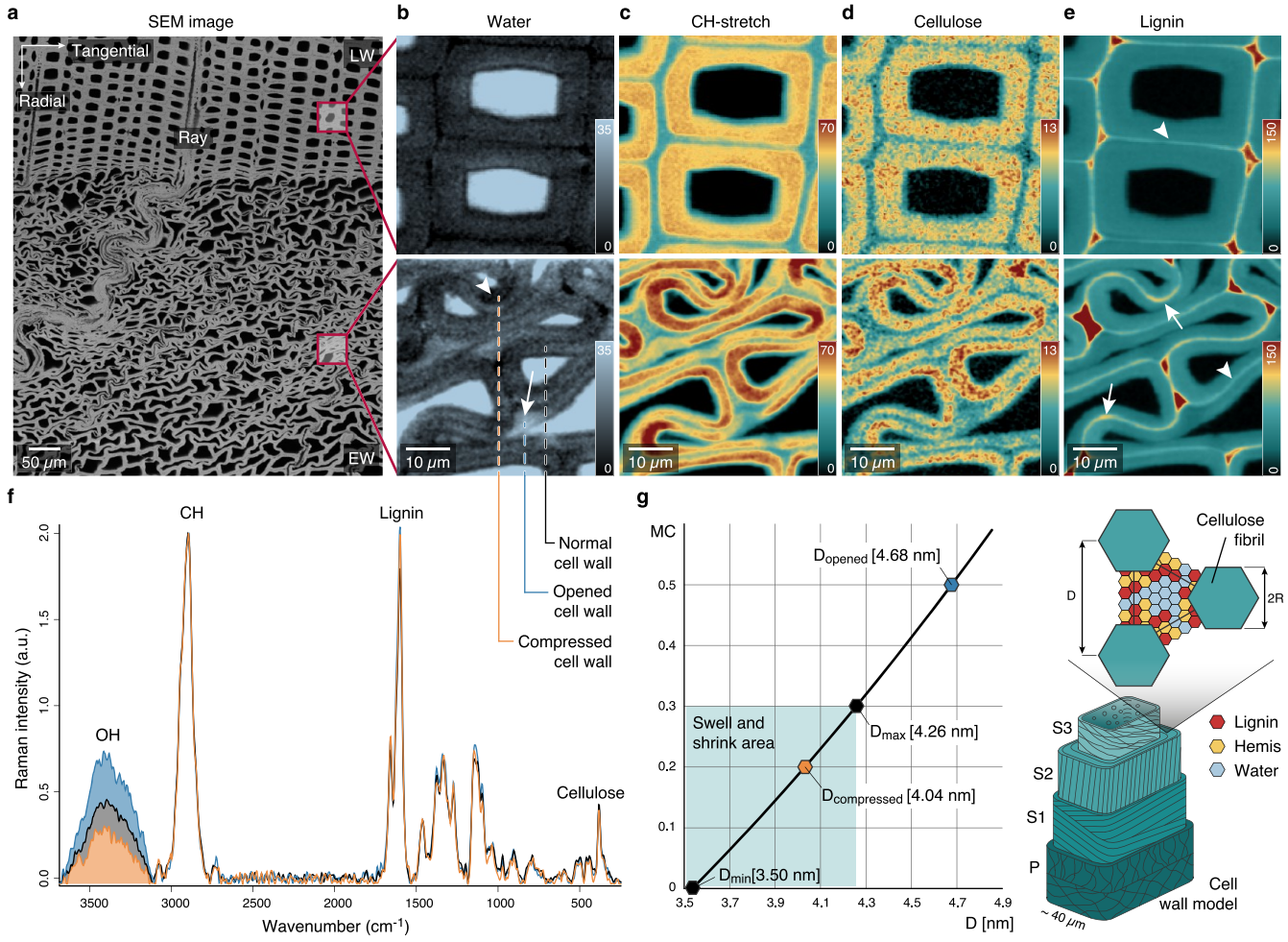

Figure 1. Raman imaging reveals changes in water content and cellulose compactness between opened and compressed cell wall areas. (a) Transverse face of the block viewed with SEM including nomenclature of wood. Early wood (EW) is highly buckled, but not the late wood (LW). (b)−(e) Raman images comparing unaltered LW cell walls with compressed EW cell walls. (b) OH integration reveals heterogeneous water distribution in EW cell walls whereas LW cells show uniform lower level water content. (c) The integration of the CH peak depicts denser regions in the cell wall with the highest curvature (dark red). (d) Raman images based on the cellulose peak 380 cm^{-1} show a heterogeneous pattern. (e) Compressed EW cells show greater lignin concentration in the middle lamella of compressed cell wall regions. Images are based on the integral range for lignin (1557−1696 cm^{-1}). (f) Average spectra of normal, opened, and compressed cell wall areas (see dashed lines in (b) bottom). (g) Distance (D) change between cellulose microfibrils based on eq 1 in Bertinetti et al.[22] (Supporting Note 2) for compressed, normal, and opened areas and schematic representation (sketch inspired by Bertinetti et al.[22]).

goes hand in hand with cell wall curvature (Supporting Note 1 and Supporting Figure 1 and 2) and the high intensity of CH-stretching, confirming a denser arrangement of cell wall polymers (Figure 1c, dark red regions). Integrating the cellulose peak at 380 cm^{-1} shows a very similar picture with high intensity in the compressed region (Figure 1d), whereas 1600 cm^{-1} integration of aromatic components shows the highest intensity between the cells (red cell corner and middle lamella) in normal and compressed wood (Figure 1e). The higher intensity of the cellulose band in the compressed cell wall areas (Figure 1d) points to a denser arrangement of cellulose microfibrils (Figure 1d). The visualized molecular differences between normal, compressed, and opened areas (Figure 1b−d) are clearly confirmed in the three extracted Raman spectra, especially in the OH-stretching region (Figure 1f). The spectrum extracted from the opened area (Figure 1f, blue line) showed the highest OH stretching band, followed by the spectrum extracted from a "normal" cell wall (Figure 1f, black) and the smallest band in the compressed area (Figure 1f, orange spectrum). The vice versa picture of low cellulose signal (Figure 1d) versus high water signal (Figure 1b) is assumed to be due to a change in the distance between microfibrils and the water between these, respectively. These distance changes between microfibrils are quantified on the basis of the equation developed to determine the cellulose nanocrystal separation based on water content.[22] We rearranged this equation (Supporting Note 2) and assumed that the cell wall of the normal (unaltered) areas is completely saturated (as measured in water). On the basis of the OH integral values (Figure 1f) the average water content was calculated for the compressed and opened region (Supporting Note 3). With a maximal distance (D_{max}) of 4.2 nm for a fully saturated cell wall and the minimum distance (D_{min}) of 3.5 nm for completely dry wood,[22] the compressed microfibril distance is 4.04 nm and widens up to 4.68 nm in the opened region (Figure 1g).

A closer look at the Raman images revealed that lignin in the middle lamella has a higher intensity in the compressed cell

https://dx.doi.org/10.1021/acs.nanolett.0c00205
Nano Lett. 2020, 20, 2647−2653

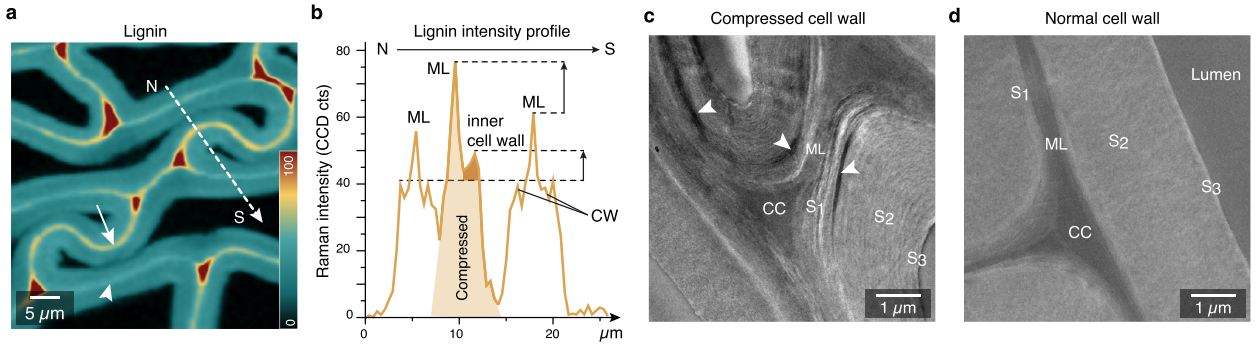

Figure 2. Compressed cell wall areas show a higher lignin content. (a) Raman image shows greater lignin concentration in the middle lamella of compressed cell wall regions (arrow) as compared to normal and widened regions (arrowhead). (b) The dashed line drawn across compressed and normal cell wall regions (in panel a) shows the lignin intensity profile. Note that the middle lamella in the compressed cell wall region (CW) has distinctly higher intensity for lignin as well as the inner compressed cell wall. (c) TEM images of compressed and (d) normal cell walls. Arrowheads indicate areas of high lignin concentration.

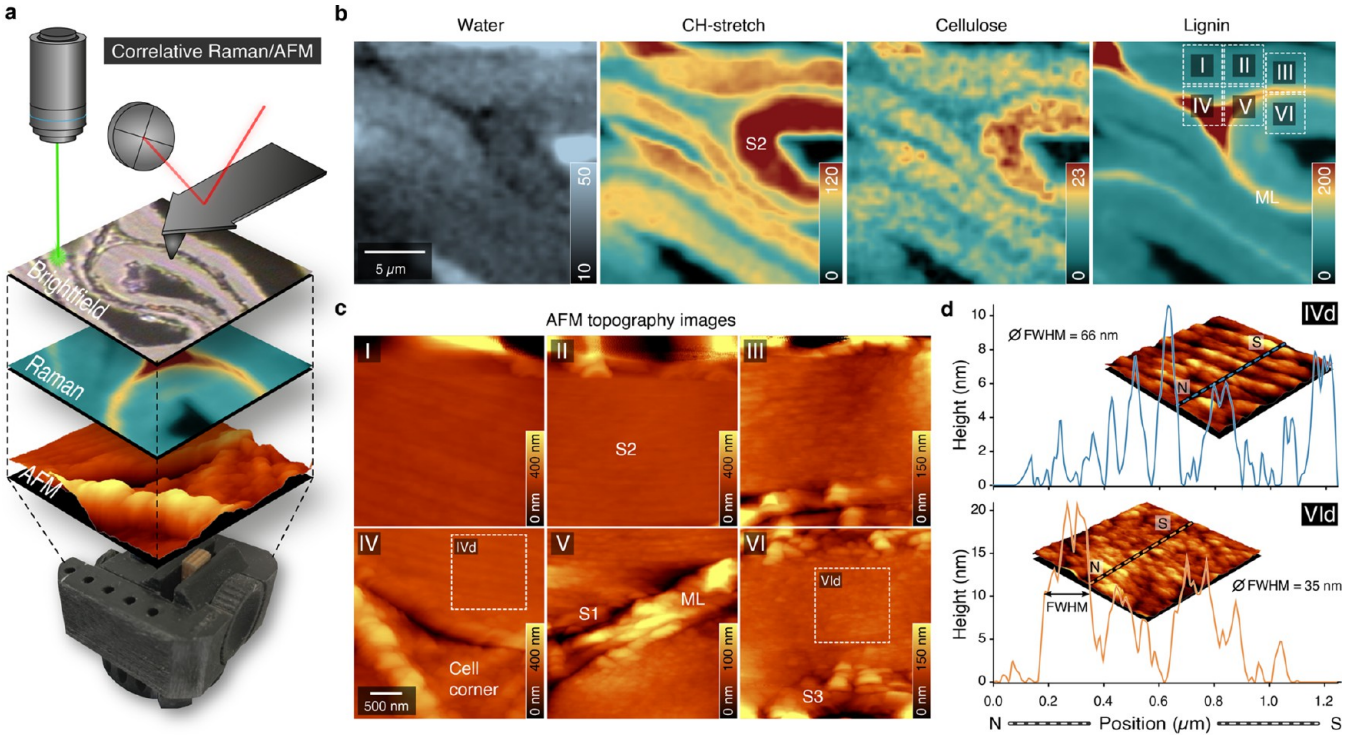

Figure 3. Correlative Raman/AFM measurements of compressed early wood of cell wall regions show microchemical and nanostructural differences. (a) Correlative approach to acquire different images exactly from the same sample positions of a wood sample compressed in a 3D printed device. The confocal Raman images visualize the chemistry in context with microstructure by acquiring the inelastic backscattering of laser light, whereas the AFM tip reaches the sample from above, providing a three-dimensional topographical view at nano resolution. (b) Raman images based on CH-stretching of all organic components (2774−3033 cm^{-1}), aromatic components (1557−1696 cm^{-1}), and components representing lignin and cellulose (342−402 cm^{-1}) reveal the compactness of the compressed inner cell wall. (c) Different AFM topographical images showing differences between outer (opened) and inner (compact) cell walls. (d) Height profiles of the opened and compressed secondary cell wall with calculated full width at half-maximum (fwhm).

wall regions (Figure 1e and Figure 2a, arrows) compared to other cell wall regions and unaltered latewood (Figure 1e and Figure 2a, arrowhead). The middle lamella seems to get thicker, and the lignin intensity profile across the "normal" and compressed cell wall confirms the lignin increase in the middle lamella and in the compressed cell wall (Figure 2b). Thus, the question raises: Is lignin "flowing" when compressing the wood sample? Water-saturated lignin in cell walls undergoes a glass transition at around 70−100 °C.[23] But there is so far no report that lignin movement (displacement) in the cell wall can also occur at ambient temperature when subjected to pressure or mechanical forces, such as compression. Besides our Raman evidence, also TEM images show intensely stained lignin patches and streaks for cell walls compressed at ambient temperature (Figure 2c). Similar patches have been reported in wood samples at higher temperatures during pulping,[24] whereas the normal cell wall area shows uniform lignin distribution (Figure 2d). In a recent NMR study it was suggested that lignin/hemicellulose interactions are much weaker[25] than has been previously suggested. This implies that lignin can migrate within the cell wall under mechanical load,

https://dx.doi.org/10.1021/acs.nanolett.0c00205
Nano Lett. 2020, 20, 2647−2653

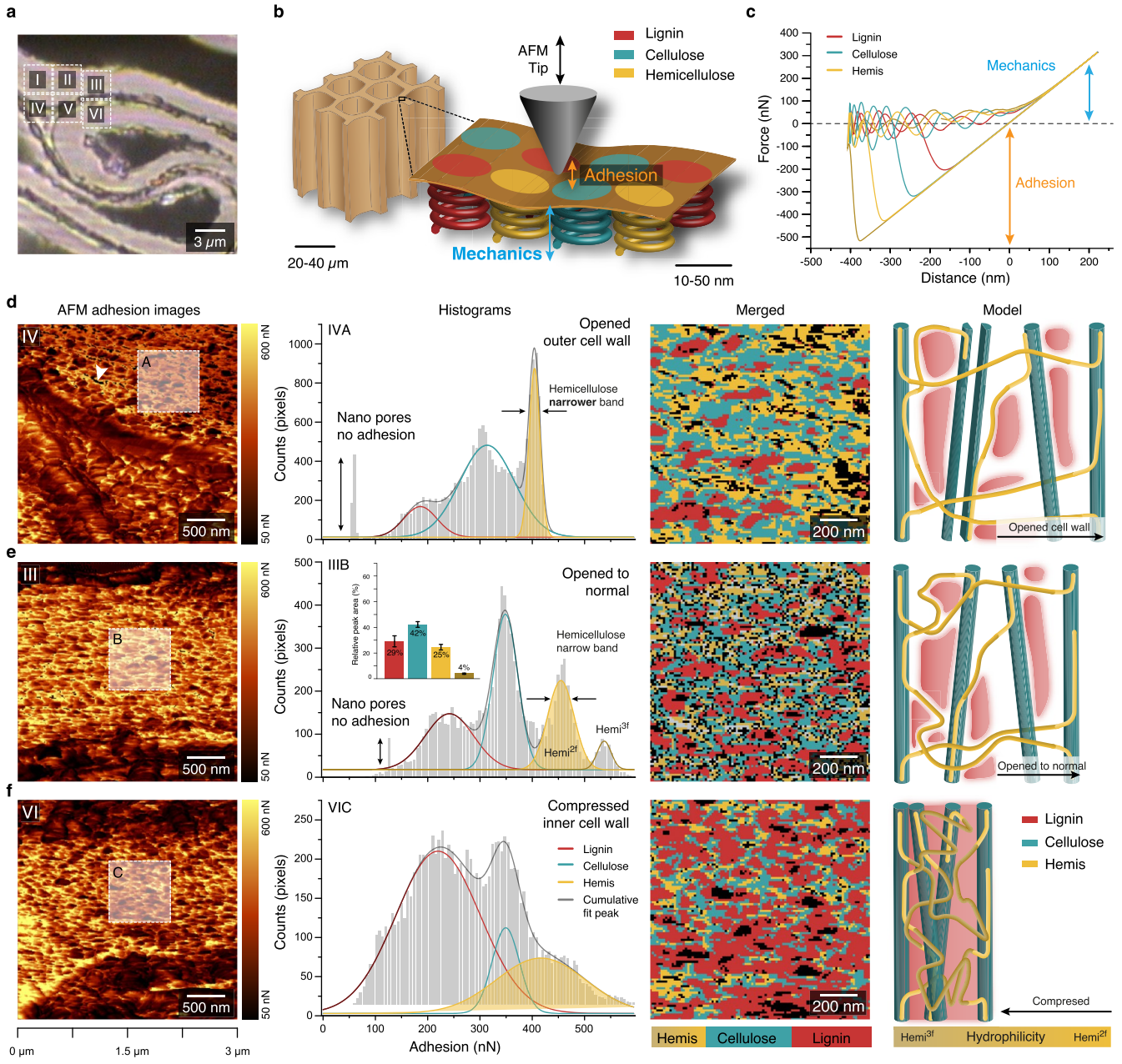

Figure 4. AFM adhesion values of compressed wood reveal nanodomains of plant cell wall polymers and their rearrangement in compressed and opened regions. (a) Bright field image with insets showing the areas scanned with AFM. (b) Schematics of AFM tip interaction with the wood polymer nanodomains within the cell wall (sketch inspired by Mandriota et al.[32]). (c) Force−distance curves representative for different cell wall components (extracted from area 3). (d)−(f) AFM adhesion images (first row) show different arrangements of nanodomains in highly opened (d, inset A), normal to opened (e, inset B), and compressed cell wall regions (f, inset C). Displaying the adhesion values as histograms results in three to four peaks representing the cell wall polymers (second row). Merged images of the different cell wall components created by extracting the pixels under the fitted curves for each component (with standard error) (third row) give their distribution, and cell wall models (inspired by Kang et al.[25]) show the relationship and arrangement of the different cell wall components, including uncoiling of the hemicellulose (fourth row). Note: The histograms in (d) and (e) show sharp and well differentiated peaks due to better accessibility in the normal to opened state. Especially in (d), unfolding of hemicelluloses due to cell wall widening causes changes in adhesion values leading to a narrowing of the hemicellulose peak and broadening of the cellulose peak.

as now evidenced by our Raman and TEM experiments (Figure 2).

To gain additionally insights into the organization and mechanical properties on the nanolevel, we aimed at correlative Raman/AFM microscopy.[18] To probe exactly the same sample and cell wall area during compression, a sample holder was designed and 3D-printed (Figure 3a). While Raman imaging gives an overview on the distribution of the molecules on the microscale (Figure 3b), AFM provides a zoom into the nanostructure (Figure 3c,d). The scanned areas (Figure 3b; see insets I−VI on the lignin image), include normal to opened areas (I, II, III, IV) as well as compressed (V, VI) regions, which is confirmed by differences in cellulose density and water content (Figure 3b). AFM topography images visualize

https://dx.doi.org/10.1021/acs.nanolett.0c00205
Nano Lett. 2020, 20, 2647−2653

the middle lamella and cell corner and show a rather flat surface within the secondary cell wall after microtome cutting (Figure 3c). A zoom into the S2 layer, however, reveals the lamellar arrangement of the S2 layer with differences in height profiles (Figure 3d, full width of half-maxima (fwhm) 66 and 35 nm for opened (IVd) and compressed area (VId), respectively). So far, AFM has been mainly applied on embedded wood samples, and besides the lamellar structure, also cellulose aggregate sizes and pore and matrix lamella width have been determined after chemical and mechanical processing.[26,27] Recently, a new AFM protocol was introduced on native wood samples to distinguish the CML, S1, and S2 based on their Young's moduli and a stiffness gradient in the transition zone S_{12}, but nanoscale details like the lamellar structure could not be detected.[15]

In this study, we also worked on native, non-embedded wood samples and focused on nanomechanics by acquiring a force−distance curve at every pixel using the digital pulsed force mode (DPFM). Including the opened and compressed region of the cell walls (Figure 4a insets) made it possible to track changes in the nanoarchitecture of the altered wood cell walls. The different wood polymers making up the wooden cell walls, lignin, cellulose, and hemicellulose (Hemis) (Figure 4b), have different mechanical and surface properties. Crystalline cellulose has a Young's modulus of about 130 GPa, whereas lignin has a modulus of roughly 3 GPa.[28] These differences are reflected in changes of the acquired force−distance curves (Figure 4c). The adhesion force between tip and the wood cell wall depends on chemical components interacting with the tip. As the silicon tip (o.d. 10 nm) used in this work has a preference for hydrophilic materials such as polysaccharides, it is possible to distinguish between the hydrophilic polysaccharides and hydrophobic lignin on the basis of AFM adhesion images (Figure 4d−f). In the most widened outer cell wall region, nanodomains and pores (arrowhead) appear more elongated and in-line with the lamella (Figure 4d, Supporting Figure 3a−c), compared to the less widened (Figure 4e) and more compact arrangement in the compressed region (Figure 4f). The corresponding histograms of the adhesion values show three to four peaks in all three regions but differ in size and shape (Figure 4d−f, second column). These peaks seem to reflect the cell wall components and may come from greater accessibility of the probe tip to opened functional groups and conformational changes during compression and widening. The relative peak area of the four peaks in the normal or less stretched region coincides with the composition of the wooden cell wall,[28] with 42% cellulose, 29% lignin, and 29% hemicellulose (Figure 4e, second column). For softwood, two different hemicelluloses are reported, glucomannan and xylan, where the xylan is in 2-fold and 3-fold configuration,[25,29] which might be reflected in the two peaks with high adhesion values. Extracting the adhesion values only from the cell corner region results in only one peak with low adhesion values (Supporting Figure 3d−f), confirming the lignin classification for the low adhesion values as the cell corner was shown to have high lignin content (Figure 3b). Plotting the distribution of the classified cell wall polymers reveals nanodomains of the three wood polymers (Figure 4d−f, third column). In the compressed state (Figure 4f), the proportion of low adhesion values are attributed to lignin increases, whereas in the more opened state, higher accessibility to hemicelluloses is observed (Figure 4d, yellow, sharp, and narrow hemicellulose peak). These changes are likely facilitated by conformational changes of hemicelluloses, interpreted as hemicellulose uncoiling into a more linear configuration,[25] as shown in the model (Figure 4d−f, fourth column). Hemicellulose conformational changes due to shear forces were already proposed in previous studies.[25,30] The "Velcro behavior" of the wood cells is explained by hemicelluloses entangling and disentangling with the rest of the matrix.[31] On the basis of adhesion force maps, we reveal for the first time intra-cell wall rearrangement of wood components on the nanolevel caused by mechanical deformation.

Besides, also stiffness and Young's modulus behavior of the outer and inner cell wall was calculated from the slope of the repulsive force signal after the tip snapped in (Figure 4c). The Young's modulus in the compressed inner cell wall is higher than that in the opened outer cell wall (Supporting Figure 4a−c), and it is in the range of values based on AFM indentation.[33] These results support the finding on the rearrangement of the cell wall polymers and water in densified wood: a stiffer compressed region is explained with denser microfibrils and accumulation of lignin, while the outer opened part is more porous and/or water filled with hemicellulose being disentangled.

Altogether, the results based on correlative CRM and AFM of the same cell wall regions provide evidence that cell wall compression causes molecular level changes at ambient temperature, such as lignin and water redistribution and conformational changes of hemicellulose. The generally accepted concept of lignin−hemicellulose interaction in the cell wall is that these cell wall components interact by forming covalent linkages.[34] However, according to a recently proposed cell wall model[25] lignin interacts with hemicelluloses via electrostatic interactions and occurs in its own nanodomains within the cell wall architecture. This supports our finding that lignin can relocate within the cell wall and the weaker electrostatic bonds can be broken if the cell wall is locally stressed. We suggest that the extreme force generated during mechanical compression of cell walls causes lignin to detach from hemicelluloses and locally migrate within the cell wall. The new fundamental knowledge of molecular behavior is useful in transformation of wood for smart material applications.

■ ASSOCIATED CONTENT

Supporting Information

The Supporting Information is available free of charge at https://pubs.acs.org/doi/10.1021/acs.nanolett.0c00205.

Supporting notes about the relationship between cell wall curvature and water content in the cell wall, calculation of the microfibril distance, and cell water content differences; figures of data for changes during wood cell wall deformation, cell wall curvature and water content, adhesion values, compression impacts on Young's modulus, and compression and recovery of dry and wet spruce blocks; materials and methods including AFM calculations (PDF)

■ AUTHOR INFORMATION

Corresponding Author

Notburga Gierlinger − *Institute for Biophysics, Department of Nanobiotechnology (DNBT), University of Natural Resources and Life (BOKU) Sciences, 1190 Vienna, Austria;*

https://dx.doi.org/10.1021/acs.nanolett.0c00205
Nano Lett. 2020, 20, 2647−2653

orcid.org/0000-0002-3699-9931;
Email: burgi.gierlinger@boku.ac.at

Authors

Martin Felhofer − *Institute for Biophysics, Department of Nanobiotechnology (DNBT), University of Natural Resources and Life (BOKU) Sciences, 1190 Vienna, Austria*

Peter Bock − *Institute for Biophysics, Department of Nanobiotechnology (DNBT), University of Natural Resources and Life (BOKU) Sciences, 1190 Vienna, Austria*

Adya Singh − *Institute for Biophysics, Department of Nanobiotechnology (DNBT), University of Natural Resources and Life (BOKU) Sciences, 1190 Vienna, Austria*

Batirtze Prats-Mateu − *Institute of Science and Technology Austria, 3400 Klosterneuburg, Austria*

Ronald Zirbs − *Institute for Biologically Inspired Materials, Department of Nanobiotechnology (DNBT), University of Natural Resources and Life Sciences, 1190 Vienna, Austria*

Complete contact information is available at: https://pubs.acs.org/10.1021/acs.nanolett.0c00205

Author Contributions

M.F. designed the project and experiments, carried out a major part of the work, analyzed the data, and prepared the figures. B.P.-M. assisted in interpreting and analyzing the AFM results. P.B. designed and constructed the 3D printed device. A.S. did the TEM work. R.Z. contributed to the discussion and completion of the manuscript. M.F., A.S., and N.G. wrote the manuscript with assistance from all authors.

Notes

The authors declare no competing financial interest.

■ ACKNOWLEDGMENTS

We thank the whole bionami research group for helpful comments (www.bionami.at). This work is supported by a fellowship of the Austrian Academy of Science (ÖAW) [24763] and the START Project [Y-728-B16] from the Austrian Science Fund (FWF) and from the European Research Council (ERC) under the European Union's Horizon 2020 research and innovation program grant agreement No. 681885.

■ REFERENCES

(1) Fang, Z.; Zhu, H.; Yuan, Y.; Ha, D.; Zhu, S.; Preston, C.; Chen, Q.; Li, Y.; Han, X.; Lee, S.; Chen, G.; Li, T.; Munday, J.; Huang, J.; Hu, L. Novel nanostructured paper with ultrahigh transparency and ultrahigh haze for solar cells. *Nano Lett.* **2014**, *14* (2), 765−73.

(2) Frey, M.; Biffi, G.; Adobes-Vidal, M.; Zirkelbach, M.; Wang, Y.; Tu, K.; Hirt, A. M.; Masania, K.; Burgert, I.; Keplinger, T. Tunable Wood by Reversible Interlocking and Bioinspired Mechanical Gradients. *Advanced science* **2019**, *6* (10), 1802190.

(3) Gan, W.; Chen, C.; Kim, H. T.; Lin, Z.; Dai, J.; Dong, Z.; Zhou, Z.; Ping, W.; He, S.; Xiao, S.; Yu, M.; Hu, L. Single-digit-micrometer thickness wood speaker. *Nat. Commun.* **2019**, *10* (1), 5084.

(4) Gronquist, P.; Wood, D.; Hassani, M. M.; Wittel, F. K.; Menges, A.; Ruggeberg, M. Analysis of hygroscopic self-shaping wood at large scale for curved mass timber structures. *Sci. Adv.* **2019**, *5* (9), eaax1311.

(5) Guo, H.; Lukovic, M.; Mendoza, M.; Schleputz, C. M.; Griffa, M.; Xu, B.; Gaan, S.; Herrmann, H.; Burgert, I. Bioinspired Struvite Mineralization for Fire-Resistant Wood. *ACS Appl. Mater. Interfaces* **2019**, *11* (5), 5427−5434.

(6) Huang, D.; Wu, J.; Chen, C.; Fu, X.; Brozena, A. H.; Zhang, Y.; Gu, P.; Li, C.; Yuan, C.; Ge, H.; Lu, M.; Zhu, M.; Hu, L.; Chen, Y. Precision Imprinted Nanostructural Wood. *Adv. Mater.* **2019**, *31* (48), No. e1903270.

(7) Luo, J.; Wang, Z.; Xu, L.; Wang, A. C.; Han, K.; Jiang, T.; Lai, Q.; Bai, Y.; Tang, W.; Fan, F. R.; Wang, Z. L. Flexible and durable wood-based triboelectric nanogenerators for self-powered sensing in athletic big data analytics. *Nat. Commun.* **2019**, *10* (1), 5147.

(8) Merk, V.; Chanana, M.; Gierlinger, N.; Hirt, A. M.; Burgert, I. Hybrid wood materials with magnetic anisotropy dictated by the hierarchical cell structure. *ACS Appl. Mater. Interfaces* **2014**, *6* (12), 9760−7.

(9) Montanari, C.; Li, Y.; Chen, H.; Yan, M.; Berglund, L. A. Transparent Wood for Thermal Energy Storage and Reversible Optical Transmittance. *ACS Appl. Mater. Interfaces* **2019**, *11* (22), 20465−20472.

(10) Zhu, H.; Jia, Z.; Chen, Y.; Weadock, N.; Wan, J.; Vaaland, O.; Han, X.; Li, T.; Hu, L. Tin anode for sodium-ion batteries using natural wood fiber as a mechanical buffer and electrolyte reservoir. *Nano Lett.* **2013**, *13* (7), 3093−100.

(11) Song, J.; Chen, C.; Zhu, S.; Zhu, M.; Dai, J.; Ray, U.; Li, Y.; Kuang, Y.; Li, Y.; Quispe, N.; Yao, Y.; Gong, A.; Leiste, U. H.; Bruck, H. A.; Zhu, J. Y.; Vellore, A.; Li, H.; Minus, M. L.; Jia, Z.; Martini, A.; Li, T.; Hu, L. Processing bulk natural wood into a high-performance structural material. *Nature* **2018**, *554* (7691), 224−228.

(12) Li, T.; Zhai, Y.; He, S.; Gan, W.; Wei, Z.; Heidarinejad, M.; Dalgo, D.; Mi, R.; Zhao, X.; Song, J.; Dai, J.; Chen, C.; Aili, A.; Vellore, A.; Martini, A.; Yang, R.; Srebric, J.; Yin, X.; Hu, L. A radiative cooling structural material. *Science* **2019**, *364* (6442), 760−763.

(13) Berglund, L. A.; Burgert, I. Bioinspired Wood Nanotechnology for Functional Materials. *Adv. Mater.* **2018**, *30* (19), No. e1704285.

(14) Agarwal, U. P. Analysis of Cellulose and Lignocellulose Materials by Raman Spectroscopy: A Review of the Current Status. *Molecules* **2019**, *24* (9), 1659.

(15) Casdorff, K.; Keplinger, T.; Burgert, I. Nano-mechanical characterization of the wood cell wall by AFM studies: comparison between AC- and QI mode. *Plant Methods* **2017**, *13*, 60.

(16) Gierlinger, N. New insights into plant cell walls by vibrational microspectroscopy. *Appl. Spectrosc. Rev.* **2018**, *53* (7), 517−551.

(17) Zhao, Y.; Man, Y.; Wen, J.; Guo, Y.; Lin, J. Advances in Imaging Plant Cell Walls. *Trends Plant Sci.* **2019**, *24* (9), 867−878.

(18) Prats-Mateu, B.; Gierlinger, N. Tip in-light on: Advantages, challenges, and applications of combining AFM and Raman microscopy on biological samples. *Microsc. Res. Tech.* **2017**, *80* (1), 30−40.

(19) Gierlinger, N.; Schwanninger, M.; Reinecke, A.; Burgert, I. Molecular Changes during Tensile Deformation of Single Wood Fibers Followed by Raman Microscopy. *Biomacromolecules* **2006**, *7* (7), 2077−2081.

(20) Zhang, T.; Tang, H.; Vavylonis, D.; Cosgrove, D. J. Disentangling loosening from softening: insights into primary cell wall structure. *Plant J.* **2019**, *100*, 1101.

(21) Chundawat, S. P.; Beckham, G. T.; Himmel, M. E.; Dale, B. E. Deconstruction of lignocellulosic biomass to fuels and chemicals. *Annu. Rev. Chem. Biomol. Eng.* **2011**, *2*, 121−45.

(22) Bertinetti, L.; Fratzl, P.; Zemb, T. Chemical, colloidal and mechanical contributions to the state of water in wood cell walls. *New J. Phys.* **2016**, *18* (8), 083048.

(23) Salmén, L. Viscoelastic properties ofin situ lignin under water-saturated conditions. *J. Mater. Sci.* **1984**, *19* (9), 3090−3096.

(24) Schmitt, U.; Singh, A. P.; Kordsachia, O.; Pohler, E. The Topochemistry of Delignification of Pinus radiata during ASAM Pulping. In *New Horizons in Wood Anatomy*; Kim, Y. S., Ed.; Chonnam National University Press: Kwangju, 2000.

(25) Kang, X.; Kirui, A.; Dickwella Widanage, M. C.; Mentink-Vigier, F.; Cosgrove, D. J.; Wang, T. Lignin-polysaccharide interactions in plant secondary cell walls revealed by solid-state NMR. *Nat. Commun.* **2019**, *10* (1), 347.

(26) Fahlén, J.; Salmén, L. On the Lamellar Structure of the Tracheid Cell Wall. *Plant Biol.* **2002**, *4* (3), 339−345.

(27) Fahlén, J.; Salmén, L. Pore and Matrix Distribution in the Fiber Wall Revealed by Atomic Force Microscopy and Image Analysis. *Biomacromolecules* **2005**, *6* (1), 433−438.
(28) Gibson, L. J. The hierarchical structure and mechanics of plant materials. *J. R. Soc., Interface* **2012**, *9* (76), 2749−66.
(29) Terrett, O. M.; Lyczakowski, J. J.; Yu, L.; Iuga, D.; Franks, W. T.; Brown, S. P.; Dupree, R.; Dupree, P. Molecular architecture of softwood revealed by solid-state NMR. *Nat. Commun.* **2019**, *10* (1), 4978.
(30) Jin, K.; Qin, Z.; Buehler, M. J. Molecular deformation mechanisms of the wood cell wall material. *Journal of the mechanical behavior of biomedical materials* **2015**, *42*, 198−206.
(31) Keckes, J.; Burgert, I.; Fruhmann, K.; Muller, M.; Kolln, K.; Hamilton, M.; Burghammer, M.; Roth, S. V.; Stanzl-Tschegg, S.; Fratzl, P. Cell-wall recovery after irreversible deformation of wood. *Nat. Mater.* **2003**, *2* (12), 810−4.
(32) Mandriota, N.; Friedsam, C.; Jones-Molina, J. A.; Tatem, K. V.; Ingber, D. E.; Sahin, O. Cellular nanoscale stiffness patterns governed by intracellular forces. *Nat. Mater.* **2019**, *18* (10), 1071−1077.
(33) Muraille, L.; Aguie-Beghin, V.; Chabbert, B.; Molinari, M. Bioinspired lignocellulosic films to understand the mechanical properties of lignified plant cell walls at nanoscale. *Sci. Rep.* **2017**, *7*, 44065.
(34) Nishimura, H.; Kamiya, A.; Nagata, T.; Katahira, M.; Watanabe, T. Direct evidence for alpha ether linkage between lignin and carbohydrates in wood cell walls. *Sci. Rep.* **2018**, *8* (1), 6538.

https://dx.doi.org/10.1021/acs.nanolett.0c00205
Nano Lett. 2020, 20, 2647−2653